This is an open access article published under a Creative Commons Attribution (CC-BY) License, which permits unrestricted use, distribution and reproduction in any medium, provided the author and source are cited.

ACS AUTHORCHOICE

JACS
JOURNAL OF THE AMERICAN CHEMICAL SOCIETY

pubs.acs.org/JACS

Communication

Large-Cavity Coronoids with Different Inner and Outer Edge Structures

Marco Di Giovannantonio,*,▽ Xuelin Yao,▽ Kristjan Eimre,▽ José I. Urgel, Pascal Ruffieux, Carlo A. Pignedoli,* Klaus Müllen,* Roman Fasel, and Akimitsu Narita*

Cite This: J. Am. Chem. Soc. 2020, 142, 12046−12050

Read Online

ACCESS | Metrics & More | Article Recommendations | Supporting Information

ABSTRACT: Coronoids, polycyclic aromatic hydrocarbons with geometrically defined cavities, are promising model structures of porous graphene. Here, we report the on-surface synthesis of C168 and C140 coronoids, referred to as [6]- and [5]coronoid, respectively, using 5,9-dibromo-14-phenylbenzo[*m*]tetraphene as the precursor. These coronoids entail large cavities (>1 nm) with inner zigzag edges, distinct from their outer armchair edges. While [6]coronoid is planar, [5]coronoid is not. Low-temperature scanning tunneling microscopy/spectroscopy and noncontact atomic force microscopy unveil structural and electronic properties in accordance with those obtained from density functional theory calculations. Detailed analysis of ring current effects identifies the rings with the highest aromaticity of these coronoids, whose pattern matches their Clar structure. The pores of the obtained coronoids offer intriguing possibilities of further functionalization toward advanced host−guest applications.

Downloaded via LIB4RI on July 17, 2020 at 18:51:52 (UTC).
See https://pubs.acs.org/sharingguidelines for options on how to legitimately share published articles.

Coronoids are macrocyclic conjugated hydrocarbons formed by circularly fused benzenoid rings, featuring a cavity.[1−3] Kekulene is a representative coronoid with a single layer of benzene rings around the cavity, belonging to the family of cycloarenes. The first synthesis of kekulene in 1978[4] provided fundamental information about the nature of macrocyclic conjugation and aromaticity, pointing out that kekulene is better represented by Clar's model rather than the so-called Kekulé structure. Other examples of cycloarenes are cyclo[*d,e,d,e,e,d,e,d,e,e*]decakisbenzene,[5] predicted to have intriguing electronic and magnetic properties,[6−9] septulene,[10] and octulene.[11] In 2016, we reported a **C216** coronoid,[1] a macrocyclic molecule with 216 sp^2 carbon atoms distributed in more than one layer of circularly fused benzene rings (Figure 1). The **C216** coronoid can also be regarded as a nanographene with a cavity arising upon removal of the central benzene ring from a **C222** nanographene (Figure 1). Detailed characterization of **C216** was compromised by its vanishing solubility, which also limited further synthetic studies of large coronoids. Very recently, Tan and co-workers reported a synthesis of mesityl-substituted **C108** coronoid, which formed molecular bilayers.[12]

On the other hand, on-surface chemistry offers an alternative method to synthesize nanographenes and to explore their structure and electronic properties via state-of-the-art scanning probe microscopy and spectroscopy.[13−15] Recently, kekulene was studied using noncontact atomic force microscopy (nc-AFM), which corroborated its structure in accordance with Clar's model.[16] Additionally, the on-surface synthesis of a **C108** coronoid (Figure 1) was achieved,[17] which represents a smaller homologue of the **C216** coronoid. However, to date, no other coronoids have been synthesized on surfaces.

Coronoids can also serve as models for graphene with nanoscale cavities, namely nanoporous graphene, which, depending on the size and structure of the pores, has intriguing electronic and magnetic properties.[18−20] Nanoporous graphene with zigzag-edge cavities stands out[21] since it is related to nanographenes and graphene nanoribbons with zigzag edges.[22,23] However, all reported coronoids have inner and outer armchair edges, and coronoids hosting a cavity with zigzag edges have never been synthesized.

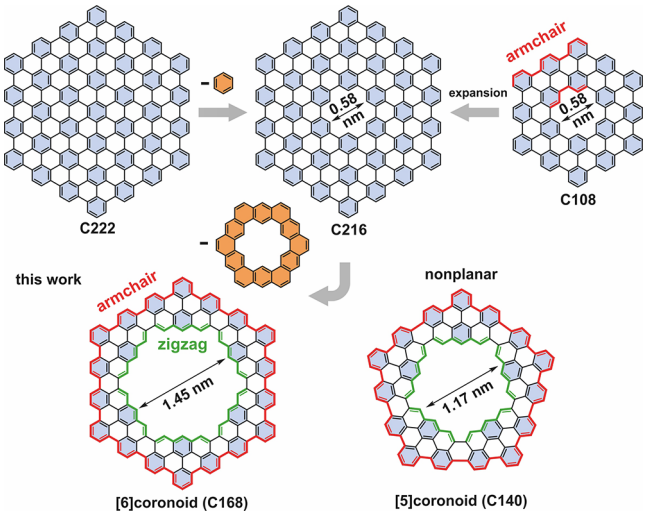

Figure 1. From nanographenes to coronoids. Clar sextets are filled in light blue. See Figure S3 for pore size determination.

Received: May 13, 2020
Published: June 26, 2020

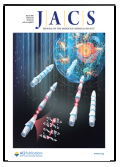

© 2020 American Chemical Society

https://dx.doi.org/10.1021/jacs.0c05268
J. Am. Chem. Soc. 2020, 142, 12046−12050

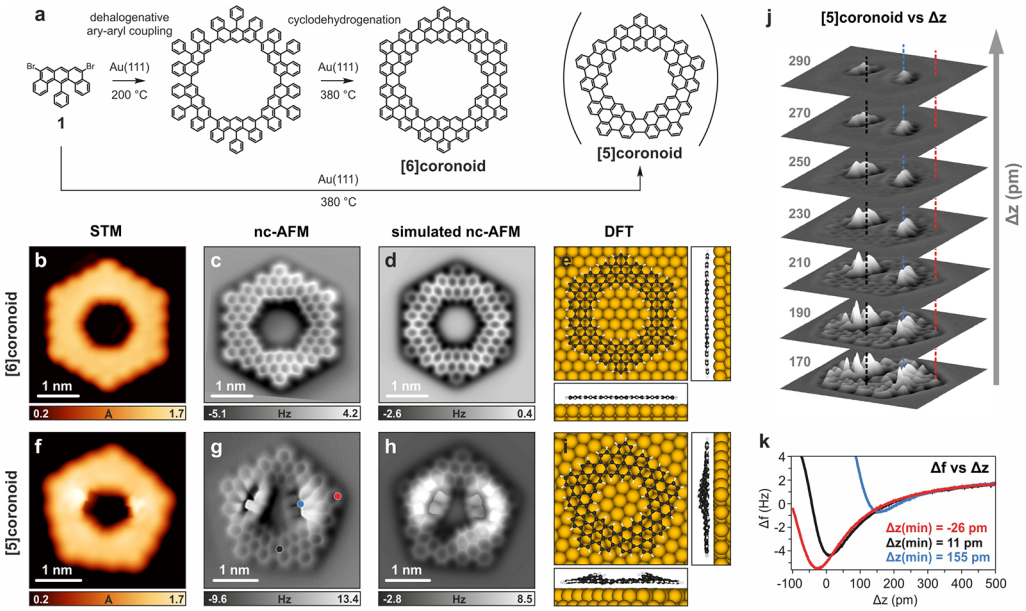

Figure 2. On-surface synthesis and characterization of [6]- and [5]coronoids. (a) Synthetic scheme. (b,f) High-resolution STM images. (c,g) nc-AFM images acquired with a CO-functionalized tip. (d,h) Simulated nc-AFM images of the DFT-optimized structures shown in panels (e,i). (j) 3D view of tip height (z) dependent nc-AFM images of [5]coronoid. (k) Frequency shift (Δf) vs Δz curves at different molecular sites (the colors of the curves correspond to those of the dots and the dashed lines in panels g and j, respectively). Scanning parameters: (b) $V_b = -20$ mV, $I_t = 100$ pA; (c) $\Delta z = +150$ Å with respect to STM set point: $V_b = -5$ mV, $I_t = 100$ pA; (f) $V_b = -20$ mV, $I_t = 100$ pA; (g) $\Delta z = +170$ Å with respect to STM set point: $V_b = -5$ mV, $I_t = 100$ pA; (j) Δz with respect to STM set point ($V_b = -5$ mV, $I_t = 100$ pA) is indicated for each layer.

In this work, we targeted an exemplary coronoid (**C168**) with outer armchair edges and a large pore (1.45 nm, C−C distance) featuring inner zigzag edges. Conceptually, this molecule can be obtained via removal of a kekulene from the aforementioned **C216** coronoid (Figure 1). Using 5,9-dibromo-14-phenylbenzo[*m*]tetraphene (**1**) as a precursor, we achieved a thermally activated on-surface synthesis of the **C168** coronoid through dehalogenative aryl−aryl coupling and subsequent cyclodehydrogenation on Au(111) (Figure 2a). **C168** is obtained by the coupling of six molecules **1** and is hereafter called [6]coronoid. The on-surface synthesis also led to the formation of a coronoid consisting of five molecules **1**, namely **C140** ([5]coronoid), which adopts a strain-driven nonplanar conformation. The on-surface structural and electronic characterization of these coronoids was performed by scanning tunneling microscopy/spectroscopy (STM/STS) and nc-AFM, which were supplemented by density functional theory (DFT) calculations supporting the experimental results and shedding light on the aromaticity of [5]- and [6]-coronoids.

For the synthesis of [6]coronoid we have designed the U-shaped precursor **1**, having a benzo[*m*]tetraphene core with a preinstalled zigzag edge as well as two bromo groups carefully positioned to allow for the macrocyclization on surface (see the SI for the synthesis of characterizations of **1**). When **1** was deposited onto a Au(111) surface held at 200 °C, the homolytic cleavage of C−Br bonds readily took place, initiating aryl−aryl coupling.[24] A temperature increase to 380 °C promoted the cyclodehydrogenation of the obtained nanostructures.[25−27] The final products of this sequence consisted of various chainlike structures, as well as some macrocyclic molecules (Figure S1) including highly symmetrical ones (Figure 2b,f). The yields of [5]- and [6]coronoids could be increased by applying high-dilution conditions,[28] with the highest yields of 30% and 6%, respectively, when the deposition rate of **1** onto Au(111) was set at 0.23 monolayer/hour (see Figure S2 for further details). The higher yield of [5]coronoid is most likely due to the ability of pentameric intermediates to undergo intramolecular head-to-tail coupling before the incorporation of the sixth building block, prevented by the high-dilution conditions.

To assess the exact chemical structure of the observed macrocycles, we acquired constant-height frequency-shift nc-AFM images using a CO-functionalized tip,[29] which clearly revealed the formation of [6]- and [5]coronoid (Figure 2c,g). [6]Coronoid is planar on the Au(111) surface and displays the expected armchair/zigzag configurations of its outer/inner edges, as further confirmed by the excellent agreement of the experimental results with simulated nc-AFM images (Figure 2d) based on the DFT-optimized structural model (Figure 2e). The size of the inner cavity is measured to be 1.40 ± 0.05 nm (C−C distance of two opposing zigzag edges), in accordance with the DFT-calculated value of 1.45 nm (see the SI for details). The [5]coronoid also reveals an armchair/zigzag configuration of outer/inner edges (Figure 2f,g), while the size of the inner cavity is reduced to 1.10 ± 0.05 nm (diameter of the inscribed circle through the central carbon atoms of the zigzag edges measured from the nc-AFM data). Again, this value agrees with the pore size of 1.09 nm estimated from the DFT-optimized geometry of the [5]coronoid on Au(111) (Figure 2i). For the [5]coronoid, two out of five inner edges appear as brighter/higher features in both the STM and nc-AFM images (Figure 2f,g). Such a nonplanar structure is in line with a partial flattening of the more distorted gas-phase geometry of [5]coronoid (Figure S3b) upon adsorption. For quantification, we acquired z-dependent nc-AFM images (Figure 2j) and recorded the frequency shift (Δf) of the CO-functionalized tip while it approached the molecule to a specific location (Figure 2k). This allowed us to extract a height difference between the highest (blue) and lowest (red)

https://dx.doi.org/10.1021/jacs.0c05268
J. Am. Chem. Soc. 2020, 142, 12046−12050

part of the molecule of 180 ± 10 pm, in good agreement with a DFT-calculated value of 170 pm (determined from the optimized geometry in Figure 2i). This height difference is substantially smaller than the value calculated for the [5]coronoid in the gas phase (360 pm, Figure S3b), which reflects the effect of van der Waals interactions with the Au(111) surface upon flattening the molecule.

To characterize the electronic properties of the [5]- and [6]coronoids, we performed constant-height differential conductance dI/dV measurements and constant-current dI/dV mappings at the detected positive (PIR) and negative ion resonances (NIR) (Figure 3a–j). Gas-phase orbital calculations (Figure 3k) show for [6]- and [5]coronoid, respectively, 6 and 5 close-lying frontier orbitals both for occupied and unoccupied levels. This is reflected in DFT calculations of the molecules on Au(111), where both the HOMO and LUMO are hybridized with the respective close-lying molecular orbitals into singular frontier ion resonances (see Figure S4 for details) that can be assigned to the experimentally measured PIR and NIR signatures. Hence, the experimental HOMO–LUMO gaps of the [6]- and [5]-coronoids on Au(111) are 2.2 and 2.5 eV, respectively. DFT calculations predicted the gas-phase HOMO–LUMO gaps of the [5]- and [6]coronoid, **C216** and **C222**, to be 2.30, 2.25, 2.15, and 1.77 eV, respectively (Figure 3k), highlighting the trend of increasing gap with increasing pore size and decreasing number of carbon atoms.

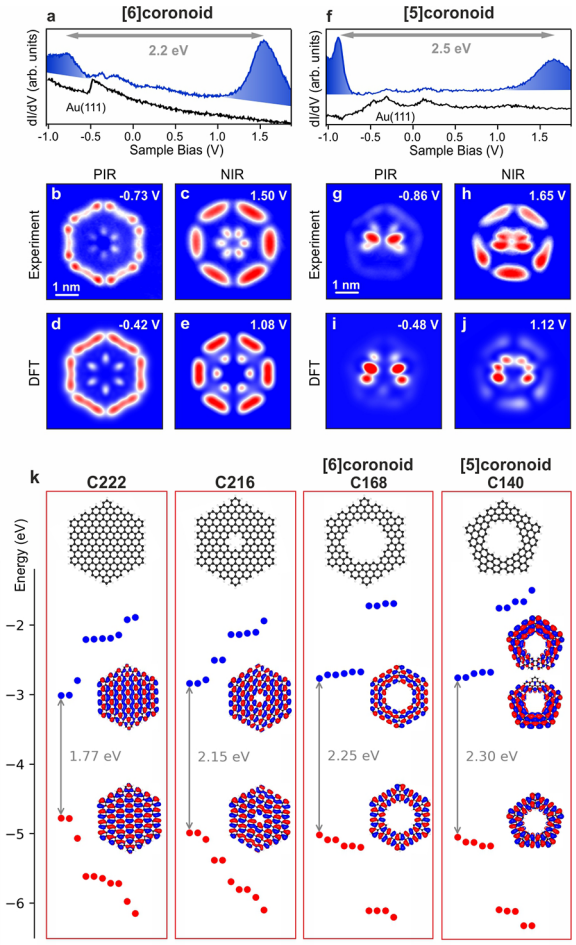

Figure 3. Differential conductance measurements and DFT simulations of [6]- and [5]coronoids. (a,f) dI/dV spectra. (b,c,g,h) dI/dV maps. (d,e,i,j) DFT-calculated local density of states at the frontier PDOS peaks (see Figure S4) of the two systems on Au(111) at the PBE level of theory. (k) Gas phase electronic characterization of the four indicated systems at the B3LYP/6-311+G** level of theory. The red and blue dots represent the occupied and unoccupied states, respectively The HOMO and LUMO wave functions are displayed. For the [5]coronoid, the LUMO is doubly quasidegenerate and both orbitals are shown.

The [6]coronoid could potentially constitute a building block for extended nanoporous graphene with larger cavities than those reported so far[20,30−32] and thus be of interest in the framework of graphene antidot lattices.[33] We calculated the electronic properties of such hypothetical periodic layer via tight binding (TB) simulations (see Figure S5 for details), which reveal a band gap of 0.63 eV (between frontier bands localized at each cavity rim), considerably reduced compared to the [6]coronoid HOMO–LUMO gap (TB) of 1.51 eV.

Carbon macrocycles are known to have peculiar aromaticity properties, leading to intriguing concepts, such as super-aromaticity,[7,34] and represent an ideal playground for studying fundamental aspects of the π-electron clouds. To display the aromaticity pattern of the [6]- and [5]coronoid, we performed nucleus-independent chemical shift (NICS) calculations at 1 Å above the center of each carbon ring ($NICS_{zz}(1)$, Figure 4a,d). The results qualitatively match between similar locations of [6]- and [5]coronoids, indicating that the nonplanarity of the

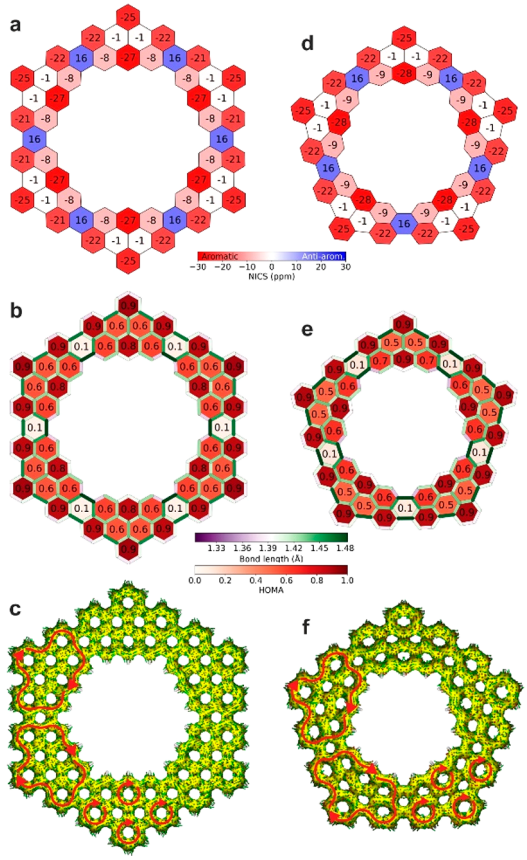

Figure 4. Aromaticity of [6]- and [5]coronoid. (a,d) $NICS_{zz}(1)$ patterns. (b,e) HOMA analysis. (c,f) ACID analysis (isovalue 0.05 au) and currents induced in the delocalized electrons. Red arrows show diatropic currents. All calculations performed at the B3LYP/6-311+G**//B3LYP/6-311G** level of theory.

https://dx.doi.org/10.1021/jacs.0c05268
J. Am. Chem. Soc. 2020, 142, 12046−12050

latter does not significantly affect its aromaticity. Moreover, the $NICS_{zz}(1)$ patterns resemble the Clar structure of these coronoids (compare Figures 1 and 4), with each Clar sextet showing strong aromatic character (from −22 ppm to −27 ppm), similar to benzene (−29 ppm). The hexagons connecting the aromatic phenanthro[2,3,4,5-*pqrab*]perylene substructures (at the "bridges" between the fused precursor units) exhibit positive NICS value (16 ppm, Figure 4a,d) reminiscent of perylene.[35] In this regard, the [6]- and [5]coronoids can be well represented by alternatingly fused perylene and pyrene constituents (Figure S6). To shed further light on the observed aromaticity pattern, we performed a harmonic oscillator model of aromaticity (HOMA) analysis (Figure 4b,e), which qualitatively matches the $NICS_{zz}(1)$ patterns of [6]- and [5]coronoid. Further, we studied the induced currents due to an applied magnetic field by analyzing the anisotropy of the induced current density (ACID) (Figure 4c,f). The valence electrons are delocalized throughout the [6]- and [5]coronoids. Each phenanthro[2,3,4,5-*pqrab*]-perylene substructure displays a macroscopic diatropic current on its outer edge (red arrows in Figure 4c,f). Within these substructures, the most aromatic sextets exhibit local diatropic currents.

In conclusion, we have achieved the successful on-surface synthesis of large, planar [6]- and nonplanar [5]coronoids featuring outer armchair and inner zigzag edges. Our study provides a complete characterization of their fundamental structural and electronic properties, revealing a HOMO−LUMO gap of 2.2 and 2.5 eV on Au(111), respectively. Both coronoids present similar aromaticity pattern and homogeneously distributed π-electron clouds, and the location of the most aromatic sextets matches their Clar structure. The [6]- and [5]coronoid have unprecedentedly large pores of 1.40 ± 0.05 and 1.10 ± 0.05 nm, respectively. Our synthetic strategy opens new avenues toward coronoids with diversified outer and inner edge structures and offers a rich playground to investigate fundamental electronic properties of coronoids. Further, lateral fusion of these coronoids potentially leads to nanoporous graphene.

■ ASSOCIATED CONTENT

Supporting Information

The Supporting Information is available free of charge at https://pubs.acs.org/doi/10.1021/jacs.0c05268.

Methods, precursor synthesis and characterizations, additional computational details, and additional experimental and theoretical results (PDF)

■ AUTHOR INFORMATION

Corresponding Authors

Marco Di Giovannantonio − *Empa, Swiss Federal Laboratories for Materials Science and Technology, nanotech@surfaces Laboratory, 8600 Dübendorf, Switzerland;* orcid.org/0000-0001-8658-9183; Email: marco.digiovannantonio@empa.ch

Carlo A. Pignedoli − *Empa, Swiss Federal Laboratories for Materials Science and Technology, nanotech@surfaces Laboratory, 8600 Dübendorf, Switzerland;* orcid.org/0000-0002-8273-6390; Email: carlo.pignedoli@empa.ch

Klaus Müllen − *Max Planck Institute for Polymer Research, 55128 Mainz, Germany; Institute of Physical Chemistry, Johannes Gutenberg University Mainz, 55128 Mainz, Germany;* orcid.org/0000-0001-6630-8786; Email: muellen@mpip-mainz.mpg.de

Akimitsu Narita − *Max Planck Institute for Polymer Research, 55128 Mainz, Germany; Organic and Carbon Nanomaterials Unit, Okinawa Institute of Science and Technology Graduate University, Okinawa 904-0495, Japan;* orcid.org/0000-0002-3625-522X; Email: narita@mpip-mainz.mpg.de

Authors

Xuelin Yao − *Max Planck Institute for Polymer Research, 55128 Mainz, Germany*

Kristjan Eimre − *Empa, Swiss Federal Laboratories for Materials Science and Technology, nanotech@surfaces Laboratory, 8600 Dübendorf, Switzerland;* orcid.org/0000-0002-3444-3286

José I. Urgel − *Empa, Swiss Federal Laboratories for Materials Science and Technology, nanotech@surfaces Laboratory, 8600 Dübendorf, Switzerland;* orcid.org/0000-0001-7608-2979

Pascal Ruffieux − *Empa, Swiss Federal Laboratories for Materials Science and Technology, nanotech@surfaces Laboratory, 8600 Dübendorf, Switzerland;* orcid.org/0000-0001-5729-5354

Roman Fasel − *Empa, Swiss Federal Laboratories for Materials Science and Technology, nanotech@surfaces Laboratory, 8600 Dübendorf, Switzerland; Department of Chemistry and Biochemistry, University of Bern, 3012 Bern, Switzerland;* orcid.org/0000-0002-1553-6487

Complete contact information is available at: https://pubs.acs.org/10.1021/jacs.0c05268

Author Contributions

[∇]M.D.G., X.Y., and K.E. contributed equally.

Notes

The authors declare no competing financial interest.

■ ACKNOWLEDGMENTS

This work was supported by the Swiss National Science Foundation under Grant No. 200020_182015, the NCCR MARVEL funded by the Swiss National Science Foundation (51NF40-182892), the Max Planck Society, the European Union's Horizon 2020 research and innovation program under Grant Agreement No. 785219 (Graphene Flagship Core 2), and the Office of Naval Research BRC Program. Computational support from the Swiss Supercomputing Center (CSCS) under Project ID s904 is gratefully acknowledged. We are thankful to E. Paenurk and R. Gershoni-Poranne for fruitful discussion on aromaticity calculations and Lukas Rotach (Empa) for his excellent technical support during the experiments.

■ REFERENCES

(1) Beser, U.; Kastler, M.; Maghsoumi, A.; Wagner, M.; Castiglioni, C.; Tommasini, M.; Narita, A.; Feng, X.; Müllen, K. A C216-Nanographene Molecule with Defined Cavity as Extended Coronoid. *J. Am. Chem. Soc.* **2016**, *138* (13), 4322−4325.

(2) Cyvin, S. J.; Brunvoll, J.; Cyvin, B. N. *Theory of Coronoid Hydrocarbons*; Springer Science & Business Media, 2012.

(3) Miyoshi, H.; Nobusue, S.; Shimizu, A.; Tobe, Y. Non-Alternant Non-Benzenoid Kekulenes: The Birth of a New Kekulene Family. *Chem. Soc. Rev.* **2015**, *44* (18), 6560−6577.

(4) Diederich, F.; Staab, H. A. Benzenoid versus Annulenoid Aromaticity: Synthesis and Properties of Kekulene. *Angew. Chem., Int. Ed. Engl.* **1978**, *17* (5), 372−374.

(5) Funhoff, D. J. H.; Staab, H. A. Cyclo[*d.e.d.e.e.d.e.d.e.e.*]-Decakisbenzene, a New Cycloarene. *Angew. Chem., Int. Ed. Engl.* **1986**, *25* (8), 742−744.
(6) Hajgató, B.; Deleuze, M. S. Quenching of Magnetism in Hexagonal Graphene Nanoflakes by Non-Local Electron Correlation. *Chem. Phys. Lett.* **2012**, *553*, 6−10.
(7) Buttrick, J. C.; King, B. T. Kekulenes, Cycloarenes, and Heterocycloarenes: Addressing Electronic Structure and Aromaticity through Experiments and Calculations. *Chem. Soc. Rev.* **2017**, *46* (1), 7−20.
(8) Yoneda, K.; Nakano, M.; Inoue, Y.; Inui, T.; Fukuda, K.; Shigeta, Y.; Kubo, T.; Champagne, B. Impact of Antidot Structure on the Multiradical Characters, Aromaticities, and Third-Order Nonlinear Optical Properties of Hexagonal Graphene Nanoflakes. *J. Phys. Chem. C* **2012**, *116* (33), 17787−17795.
(9) Hajgató, B.; Deleuze, M. S.; Ohno, K. Aromaticity of Giant Polycyclic Aromatic Hydrocarbons with Hollow Sites: Super Ring Currents in Super-Rings. *Chem. - Eur. J.* **2006**, *12* (22), 5757−5769.
(10) Kumar, B.; Viboh, R. L.; Bonifacio, M. C.; Thompson, W. B.; Buttrick, J. C.; Westlake, B. C.; Kim, M.-S.; Zoellner, R. W.; Varganov, S. A.; Mörschel, P.; Teteruk, J.; Schmidt, M. U.; King, B. T. Septulene: The Heptagonal Homologue of Kekulene. *Angew. Chem., Int. Ed.* **2012**, *51* (51), 12795−12800.
(11) Majewski, M. A.; Hong, Y.; Lis, T.; Gregoliński, J.; Chmielewski, P. J.; Cybińska, J.; Kim, D.; Stępień, M. Octulene: A Hyperbolic Molecular Belt That Binds Chloride Anions. *Angew. Chem., Int. Ed.* **2016**, *55* (45), 14072−14076.
(12) Zhao, X.-J.; Hou, H.; Ding, P.-P.; Deng, Z.-Y.; Ju, Y.-Y.; Liu, S.-H.; Liu, Y.-M.; Tang, C.; Feng, L.-B.; Tan, Y.-Z. Molecular Defect-Containing Bilayer Graphene Exhibiting Brightened Luminescence. *Sci. Adv.* **2020**, *6* (9), No. eaay8541.
(13) Palma, C.-A.; Samorì, P. Blueprinting Macromolecular Electronics. *Nat. Chem.* **2011**, *3* (6), 431−436.
(14) Lindner, R.; Kühnle, A. On-Surface Reactions. *ChemPhysChem* **2015**, *16* (8), 1582−1592.
(15) Talirz, L.; Ruffieux, P.; Fasel, R. On-Surface Synthesis of Atomically Precise Graphene Nanoribbons. *Adv. Mater.* **2016**, *28* (29), 6222−6231.
(16) Pozo, I.; Majzik, Z.; Pavliček, N.; Melle-Franco, M.; Guitián, E.; Peña, D.; Gross, L.; Pérez, D. Revisiting Kekulene: Synthesis and Single-Molecule Imaging. *J. Am. Chem. Soc.* **2019**, *141* (39), 15488−15493.
(17) Fan, Q.; Martin-Jimenez, D.; Werner, S.; Ebeling, D.; Koehler, T.; Vollgraff, T.; Sundermeyer, J.; Hieringer, W.; Schirmeisen, A.; Gottfried, J. M. On-Surface Synthesis and Characterization of a Cycloarene: C108 Graphene Ring. *J. Am. Chem. Soc.* **2020**, *142* (2), 894−899.
(18) Dias, J. R. Structure and Electronic Characteristics of Coronoid Polycyclic Aromatic Hydrocarbons as Potential Models of Graphite Layers with Hole Defects. *J. Phys. Chem. A* **2008**, *112* (47), 12281−12292.
(19) Dias, J. R.; Aihara, J. Antiaromatic Holes in Graphene and Related Graphite Defects. *Mol. Phys.* **2009**, *107* (1), 71−80.
(20) Moreno, C.; Vilas-Varela, M.; Kretz, B.; Garcia-Lekue, A.; Costache, M. V.; Paradinas, M.; Panighel, M.; Ceballos, G.; Valenzuela, S. O.; Peña, D.; Mugarza, A. Bottom-up Synthesis of Multifunctional Nanoporous Graphene. *Science* **2018**, *360* (6385), 199−203.
(21) Yang, H.-X.; Chshiev, M.; Boukhvalov, D. W.; Waintal, X.; Roche, S. Inducing and Optimizing Magnetism in Graphene Nanomeshes. *Phys. Rev. B: Condens. Matter Mater. Phys.* **2011**, *84* (21), 214404.
(22) Mishra, S.; Beyer, D.; Eimre, K.; Kezilebieke, S.; Berger, R.; Gröning, O.; Pignedoli, C. A.; Müllen, K.; Liljeroth, P.; Ruffieux, P.; Feng, X.; Fasel, R. Topological Frustration Induces Unconventional Magnetism in a Nanographene. *Nat. Nanotechnol.* **2020**, *15* (1), 22−28.
(23) Ruffieux, P.; Wang, S.; Yang, B.; Sánchez-Sánchez, C.; Liu, J.; Dienel, T.; Talirz, L.; Shinde, P.; Pignedoli, C. A.; Passerone, D.; Dumslaff, T.; Feng, X.; Müllen, K.; Fasel, R. On-Surface Synthesis of Graphene Nanoribbons with Zigzag Edge Topology. *Nature* **2016**, *531* (7595), 489−492.
(24) Di Giovannantonio, M.; Deniz, O.; Urgel, J. I.; Widmer, R.; Dienel, T.; Stolz, S.; Sánchez-Sánchez, C.; Muntwiler, M.; Dumslaff, T.; Berger, R.; Narita, A.; Feng, X.; Müllen, K.; Ruffieux, P.; Fasel, R. On-Surface Growth Dynamics of Graphene Nanoribbons: The Role of Halogen Functionalization. *ACS Nano* **2018**, *12* (1), 74−81.
(25) Clair, S.; de Oteyza, D. G. Controlling a Chemical Coupling Reaction on a Surface: Tools and Strategies for On-Surface Synthesis. *Chem. Rev.* **2019**, *119* (7), 4717−4776.
(26) Cai, J.; Ruffieux, P.; Jaafar, R.; Bieri, M.; Braun, T.; Blankenburg, S.; Muoth, M.; Seitsonen, A. P.; Saleh, M.; Feng, X.; Müllen, K.; Fasel, R. Atomically Precise Bottom-up Fabrication of Graphene Nanoribbons. *Nature* **2010**, *466* (7305), 470−473.
(27) Di Giovannantonio, M.; Contini, G. Reversibility and Intermediate Steps as Key Tools for the Growth of Extended Ordered Polymers via On-Surface Synthesis. *J. Phys.: Condens. Matter* **2018**, *30*, 093001.
(28) Fan, Q.; Wang, T.; Dai, J.; Kuttner, J.; Hilt, G.; Gottfried, J. M.; Zhu, J. On-Surface Pseudo-High-Dilution Synthesis of Macrocycles: Principle and Mechanism. *ACS Nano* **2017**, *11* (5), 5070−5079.
(29) Gross, L.; Mohn, F.; Moll, N.; Liljeroth, P.; Meyer, G. The Chemical Structure of a Molecule Resolved by Atomic Force Microscopy. *Science* **2009**, *325* (5944), 1110−1114.
(30) Bieri, M.; Treier, M.; Cai, J.; Aït-Mansour, K.; Ruffieux, P.; Gröning, O.; Gröning, P.; Kastler, M.; Rieger, R.; Feng, X.; Müllen, K.; Fasel, R. Porous Graphenes: Two-Dimensional Polymer Synthesis with Atomic Precision. *Chem. Commun.* **2009**, No. 45, 6919.
(31) Jiang, D.; Cooper, V. R.; Dai, S. Porous Graphene as the Ultimate Membrane for Gas Separation. *Nano Lett.* **2009**, *9* (12), 4019−4024.
(32) Du, A.; Zhu, Z.; Smith, S. C. Multifunctional Porous Graphene for Nanoelectronics and Hydrogen Storage: New Properties Revealed by First Principle Calculations. *J. Am. Chem. Soc.* **2010**, *132* (9), 2876−2877.
(33) Pedersen, T. G.; Flindt, C.; Pedersen, J.; Mortensen, N. A.; Jauho, A.-P.; Pedersen, K. Graphene Antidot Lattices: Designed Defects and Spin Qubits. *Phys. Rev. Lett.* **2008**, *100* (13), 136804.
(34) Liu, C.; Sandoval-Salinas, M. E.; Hong, Y.; Gopalakrishna, T. Y.; Phan, H.; Aratani, N.; Herng, T. S.; Ding, J.; Yamada, H.; Kim, D.; Casanova, D.; Wu, J. Macrocyclic Polyradicaloids with Unusual Super-Ring Structure and Global Aromaticity. *Chem.* **2018**, *4* (7), 1586−1595.
(35) Fias, S.; Fowler, P. W.; Delgado, J. L.; Hahn, U.; Bultinck, P. Correlation of Delocalization Indices and Current-Density Maps in Polycyclic Aromatic Hydrocarbons. *Chem. - Eur. J.* **2008**, *14* (10), 3093−3099.

https://dx.doi.org/10.1021/jacs.0c05268
J. Am. Chem. Soc. 2020, 142, 12046−12050